J Appl Electrochem (2014) 44:45–51
DOI 10.1007/s10800-013-0590-x

RESEARCH ARTICLE

# Micro/nano-structured $SnS_2$ negative electrodes using chitosan derivatives as water-soluble binders for Li-ion batteries

**Haoxiang Zhong · Peng Zhou · Lu Yue · Daoping Tang · Lingzhi Zhang**

Received: 3 May 2013 / Accepted: 13 July 2013 / Published online: 31 July 2013


**Abstract** Micro/nano-structured $SnS_2$ was prepared by a hydrothermal method using biomolecular L-cysteine and $SnCl_4{\cdot}5H_2O$ as sulfur source and tin source, respectively. The electrochemical performances of $SnS_2$ electrodes were investigated using water-soluble binders of carboxymethyl chitosan (C-chitosan) and chitosan lactate, and compared with the conventional water-soluble sodium carboxymethyl cellulose (CMC) and non-aqueous polyvinylidene difluoride (PVDF). $SnS_2$ electrode using the water-soluble binders (C-chitosan, chitosan lactate, and CMC) showed higher initial coulombic efficiency, larger reversible capacity, and better rate capabilities than that of PVDF. In addition, $SnS_2$ electrode using C-chitosan binder exhibited somewhat worse cycling stability, but better rate capability at a high rate of 5C than CMC.

**Keywords** Micro/nano-structured $SnS_2$ · Carboxymethyl chitosan · Chitosan lactate · CMC · Li-ion batteries

H. Zhong · L. Yue · D. Tang · L. Zhang (✉)
CAS Key Laboratory of Renewable Energy, Guangzhou Institute of Energy Conversion, Chinese Academy of Sciences, Guangzhou 510640, Guangdong, China
e-mail: lzzhang@ms.giec.ac.cn

P. Zhou
South China Sea Environment Monitoring Center, State Oceanic Administration, Guangzhou 510300, Guangdong, China

L. Yue
University of Chinese Academy of Sciences, Beijing 100039, China

## 1 Introduction

Lithium-ion batteries (LIBs) are currently the most preferred energy storage devices in portable electronic devices due to the high energy density, high operating voltage, and low self-discharge [1, 2]. Electrode materials, electrolytes, and separators, as important components in LIBs, have been intensively developed in recent years [3–6]. However, the binder, as an electrochemically inactive material, which functions to bind together the active material, the conducting agent, and the current collector, has attracted less attention [7–9].

PVDF has been successfully used as a binder for both the positive and negative electrodes in commercial LIBs, but it has some critical drawbacks [10, 11]. PVDF binder is generally dissolved in the volatile, flammable, or explosive *N*-methyl-2-pyrrolidone (NMP), which poses serious pollution to the atmosphere. In addition, high cost and low flexibility of PVDF also limits its application in large-scale batteries. Therefore, the development of alternative binders with less cost and more environmental friendly feature is essential. Recently, water-soluble polymers, such as sodium carboxymethyl cellulose (CMC) [12–14], polyacrylic acid (PAA) [15, 16], and alginate [17], have been explored as binders, especially for Si negative electrode which has severe volume change of about 400 % during cycling. The hydrogen and/or covalent bonds formed between the carboxylic or hydroxyl groups of these water-soluble polymers and the silicon particles could remarkably accommodate the huge volume change, thus significantly improved the electrochemical properties of the electrodes [12, 17].

Chitosan and its derivatives are a family of natural polymers containing polar groups such as amine, carboxyl, and hydroxyl groups. But chitosan itself is insoluble in

water. By milling the mixture of silicon powder, chitosan, and carbon blacks in the water, Larcher and co-workers [18] were able to prepare Si negative electrode, which showed fairly moderate electrochemical performances. Similar to Si, $SnS_2$ as an anode material has high theoretical capacity of 645 mAh $g^{-1}$, and also suffers from the severe volume changes (up to 300 %) during cycling [19–25].

In this paper, we synthesized a micro/nano-structured $SnS_2$ using biomolecular L-cysteine and $SnCl_4{\cdot}5H_2O$ as sulfur source and tin source, respectively. The electrochemical performances of $SnS_2$ electrodes were studied using water soluble binders of C-chitosan and chitosan lactate, compared with the conventional binders of CMC and PVDF.

## 2 Experimental

### 2.1 Chemicals and materials

L-cysteine and $SnCl_4{\cdot}5H_2O$ were purchased from Guangzhou Chemical Reagent Factory (China). PVDF (Solvay Solef®6020) was from Shenzhen Micro Electron Co., LTD (China), C-chitosan and chitosan lactate (viscosity = 10–80 mpa s) were both purchased from AOKANG Chemical Reagent (China); CMC (viscosity = 800–1200 mpa s) was obtained from Sigma-Aldrich. Chemical structures of the polymers mentioned above were shown in Table 1.

**Table 1** The chemical structures of four polymer binders

| Name | Structure |
|---|---|
| C-chitosan | 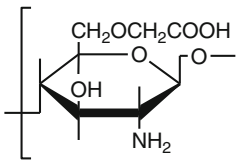 |
| Chitosan lactate | 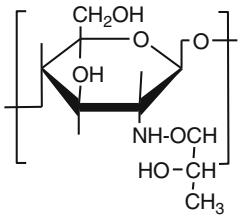 |
| CMC | 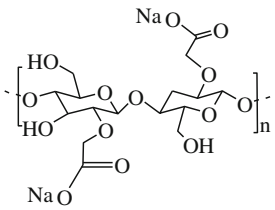 |
| PVDF | 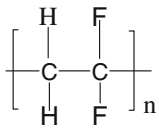 |

### 2.2 Preparation of micro/nano-structured $SnS_2$

Micro/nano-structured $SnS_2$ was synthesized through a modified procedure reported before [26]. In a typical synthesis, L-cysteine ($C_3H_7NS$, 0.25 g, 2.1 mmol) and $SnCl_4{\cdot}5H_2O$ (0.35 g, 1 mmol) were dissolved in deionized water (40 mL). After being stirred for 10 min, the mixture was transferred into a Teflon-lined autoclave (50 mL), and incubated in an electric oven at 180 °C for 24 h. The autoclave was then removed from the oven and cooled down to room temperature. The yellow precipitate was collected by centrifugation, washed with deionized water and ethanol, and finally dried at 80 °C for 12 h.

### 2.3 Physicochemical characterization

The morphologies of the as-prepared $SnS_2$ were observed by a SEM (Hitachi S-4800, Japan) equipped with an energy-dispersive detector (EDS) and TEM (JEOL JEM 2100 F, Japan) images with electron diffraction patterns. The phase identification was performed by X-ray diffraction (XRD, PANALYTICAL Incorporated, the Netherlands) from 10° to 80° with a CuKa source ($\lambda = 0.154178$ nm). Raman spectroscopy was carried out to monitor the variations in the sample using a HR800 Confocal Raman system (HORIBA Jobin-Yvon, France) with 532 nm diode Laser excitation on a 300 lines/mm grating at room temperature. The specific surface area was calculated using the Brunauer–Emmet–Teller (BET) method, and the Barrett–Joyner–Halenda (BJH) pore size distribution was determined using the desorption branch of the isotherm (SI-MP-10/PoreMaster 3, Quanatachrome Instruments, America).

### 2.4 Electrochemical measurements

$SnS_2$ was used as active material, carbon black (CB) as the conductive agent and C-chitosan (3.5 wt%) and chitosan lactate (3.5 wt%) aqueous solution are used as the binder, respectively. Measured amounts of $SnS_2$, CB, and C-chitosan (chitosan lactate) were mixed according to 75 wt% active material, 15 wt% CB, and 10 wt% binder. The slurry was coated onto a copper foil and dried in a vacuum oven at 110 °C for 12 h to remove the water solvent. To compare the effect of the binders on electrochemical performance, 12 wt% PVDF solution in *N*-methyl pyrrolidinone (NMP), and 3.5 wt% CMC aqueous solution were used as the binders for $SnS_2$,

respectively. The coin cells (CR2025) were assembled to test the electrochemical performance of the as-prepared $SnS_2$, using 1 M $LiPF_6$ EC/DEC (1:1 by volume) as the electrolyte, a microporous membrane (Celguard 2400, USA) as the separator. The cells were charged and discharged galvanostatically in the fixed voltage window from 0 mV to 2.0 V (versus $Li^+/Li$) on a Shenzhen Neware battery tester (China) at 25 °C. Cyclic voltammetry (2.0–0 V, 0.2 mV $s^{-1}$) was performed by using an electrochemical workstation (Zennium/IM6, Germany). The rate capability was evaluated by varying the rate from 0.5 to 5C. Electrochemical impedance spectroscopy (EIS) was measured with electrochemical workstation (Zennium/IM6, Germany) by applying an alternating voltage of 5 mV over the frequency ranging from $10^{-2}$ to $10^5$ Hz.

## 3 Results and discussion

### 3.1 Structure and composition characterization

The crystallographic structure and phase purity of the as-prepared samples were examined by XRD (Fig. 1a). All the peaks of the sample in the XRD pattern can be readily indexed to a pure hexagonal phase of $SnS_2$ in good agreement with the reported values (JCPDS card, No. 23-0677) [27]. No peaks of other phases were detected, indicating the high purity of the as-synthesized product. Raman spectrum was used to further confirm the composition of the sample. The Raman spectrum of the prepared $SnS_2$ showed an intense peak at about 311 $cm^{-1}$ (Fig. 1b), which was attributed to the A1g mode of $SnS_2$ according to the group theory analysis by previous studies [28, 29].

The morphologies and structures of the prepared samples were examined by SEM and TEM (Fig. 2). The low magnification SEM image showed that $SnS_2$ with uniformed spherical morphologies were observed. The magnified SEM image revealed an interesting phenomenon that $SnS_2$ had a uniformed 3D micro/nano structure with an average diameter of 2.0 μm, which was assembled by many interleaving and slightly bending nanoflakes with a thickness less than 30 nm (Fig. 2a, b). TEM images of $SnS_2$ confirmed the highly dispersed micro/nano structure (Fig. 2c). The corresponding electron diffraction pattern (inset in Fig. 2c), taken under the electron beam perpendicular to the surface of a nanosheet, could be indexed as a hexagonal phase $SnS_2$ along the [001] axis. The magnified image showed clearly the lattice stripe of the nanoplate with the interplanar distance of 0.59 nm between the neighboring lattices which is consistent with the (001) planes of a hexagonal phase $SnS_2$ (Fig. 2d).

### 3.2 BET surface area

Nitrogen gas adsorption–desorption isotherms and Barrett–Joyner–Halenda (BJH) characterization were used to measure specific surfaces areas (SSA)and the pore size distribution of the hierarchical flowerlike $SnS_2$ (Fig. 3). The type-IV isotherm with a hysteresis loop in the range of 0.4–1.0 *P*/*P*0 was in accordance with the assembled plate-like structure [30, 31]. The quantitative calculation showed that the as-prepared $SnS_2$ sample had a surface area of 78.4 $m^2$ $g^{-1}$. The pore size distribution of the $SnS_2$ sample was shown in Fig. 3b. Two different mesopore sizes of 4.3 nm and 13.0 nm were observed, which offered a high surface area and thus avoided the permanent trapping of lithium ions that is possible with micropores [32].

### 3.3 Electrochemical performance

Cyclic voltammetry of $SnS_2$ electrode using C-chitosan binder was performed between 0.0 and 2.0 V at a scan rate of 0.2 mV $s^{-1}$ (Fig. 4). Two broad peaks at about 1.1 and 0.8 V in the first potential sweeping process disappeared in the second run, due to the transformation of $SnS_2$ nanosheets to metallic tin and $Li_2S$ (Eq. 1) [33, 34]. In the more cathodic potential range of 0.1–0.5 V, a broad peak at

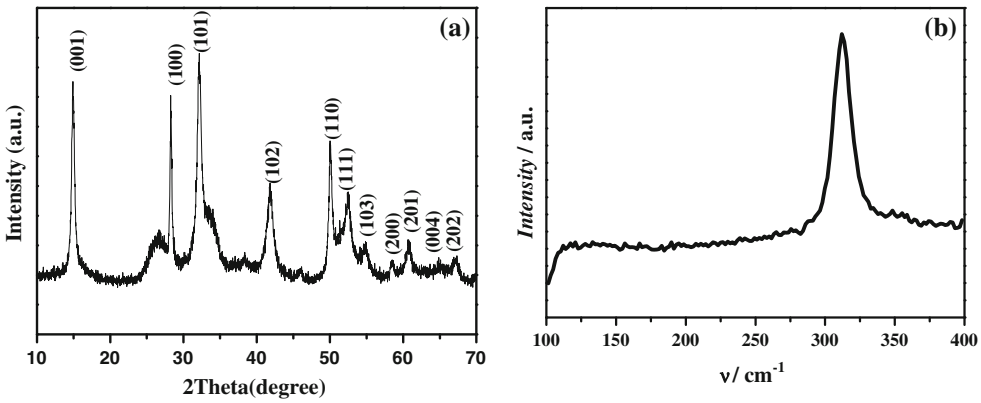


**Fig. 1** **a** XRD pattern and **b** Raman spectrum of the prepared $SnS_2$ sample

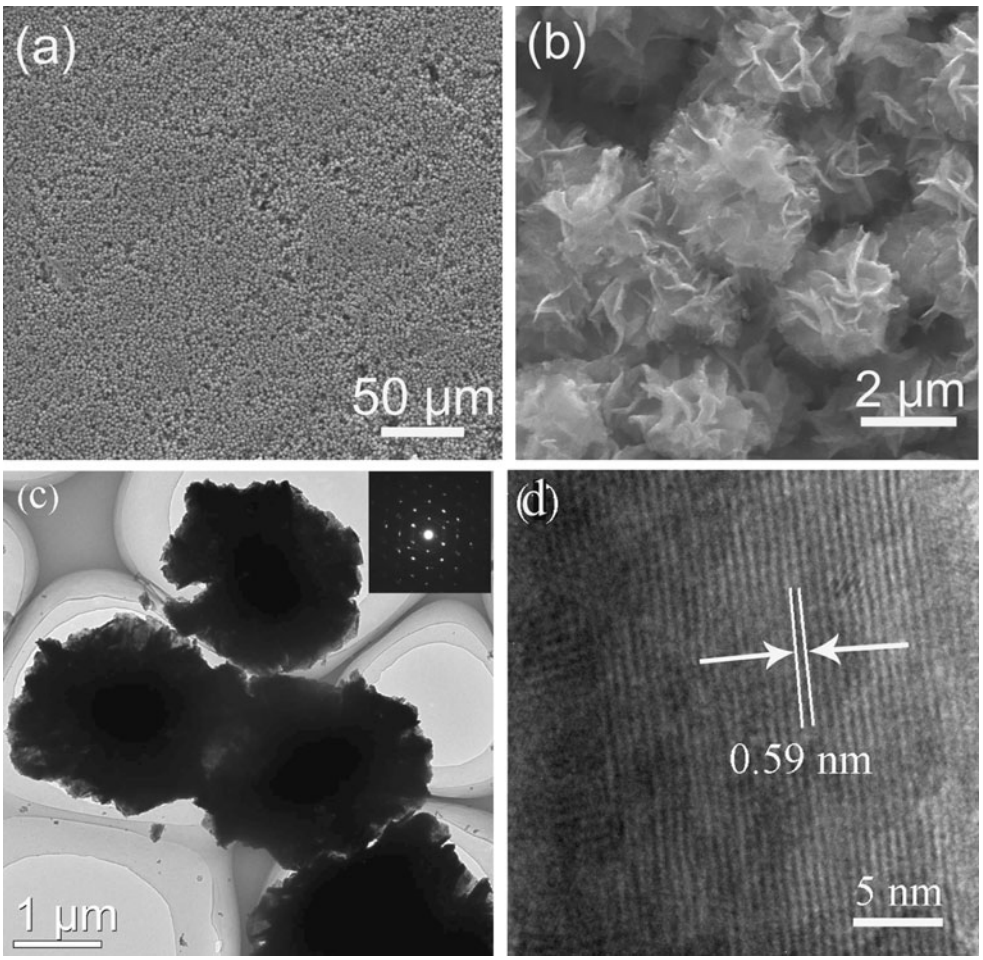


**Fig. 2** Morphologies of the as-synthesized $SnS_2$. **a**, **b** SEM images of the micro/nano– structured $SnS_2$ prepared using the hydrothermal method; **c** TEM image of $SnS_2$, *inset* showing the corresponding electron diffraction pattern; **d** HRTEM image of the micro/nano-structured $SnS_2$

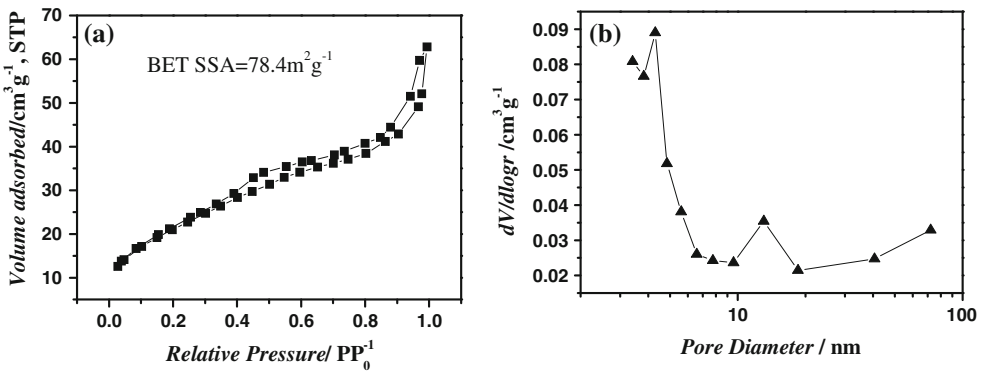


**Fig. 3** **a** $N_2$ adsorption–desorption isotherm and **b** pore size distribution curves of $SnS_2$

about 0.1 V in the first cathodic sweep was observed, which originated from the reaction of Li ions and Sn metal (Eq. 2). For the following cycles, the intercalation of lithium ions from Sn occurred in the potential range of 0.0–0.5 V and their deintercalation occurred in the potential range of 0.5–0.7 V. The additional peak at 1.9 V could be attributed to the lithium intercalation of the $SnS_2$ layers without phase decomposition [34, 35].

$$SnS_2 + 4Li \rightarrow Sn + 2Li_2S \quad (1)$$

$$Sn + 4.4Li \leftrightarrow Li_{4.4}Sn \quad (2)$$

Micro/nano-structured $SnS_2$ using C-chitosan, chitosan lactate or CMC binder exhibit a higher specific capacity than that of PVDF. The first charge–discharge profiles of $SnS_2$ electrodes cycled between 2.0 V and 0.0 v at 0.5C showed that $SnS_2$ electrodes using C-chitosan, chitosan

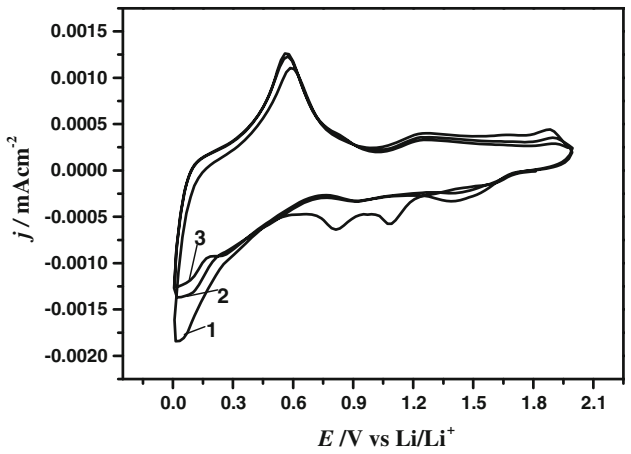


**Fig. 4** Cyclic voltammetry for micro/nano-structured $SnS_2$ using C-chitosan binder for the first three cycles from 2.0 to 0 V versus $Li/Li^+$

lactate, CMC, and PVDF binder delivered a first discharge capacity of 899, 806, and 937 and 661 mAh $g^{-1}$, respectively (Fig. 5a). After 50 cycles, $SnS_2$ electrode maintained a discharge specific capacity of 479 mAh $g^{-1}$ (C-chitosan), 488 mAh $g^{-1}$ (Chitosan lactate), 544 mAh $g^{-1}$(CMC), and 265 mAh $g^{-1}$ (PVDF), respectively (Fig. 5b). High coulombic efficiency (CE) is critical for practical applications and is challenging to achieve for Sn-based anodes with huge volume change due to the need to maintain a stable SEI layer [24]. $SnS_2$ electrode using C-chitosan, chitosan lactate, CMC binder showed higher initial coulombic efficiency (ICE) than PVDF; 47.5, 62.1, 61.0, and 60.8 % for PVDF, CMC, C-chitosan, and Chitosan lactate, respectively. The rate capability (from 0.1 to 5C) of micro/nano-structured $SnS_2$ using different binders was also studied (Fig. 5c). $SnS_2$ electrode using water soluble binders (e.g., C-chitosan, chitosan lactate, or CMC) displayed better rate capability than PVDF. Even at higher rates, such as 5C, $SnS_2$ electrode using C-chitosan, chitosan lactate, CMC, and PVDF binder, delivered a higher specific capacity of 458, 432, and 442 mAh $g^{-1}$, respectively, as compared with 175 mAh $g^{-1}$ for PVDF.

We analyzed the impact of the chemical structures of four binders on electrochemical performances (Table 1). Apparently, the water-soluble binders contain various kinds of polar groups such as carboxy, hydroxyl, or amine group in their chemical structures when compared with PVDF. These polar groups can ensure better interfacial interaction through hydrogen and/or covalent bonds with $SnS_2$ [12, 17], and the amine groups from chitosan derivatives, could possibly act as an acid scavenger (HF generated from the decomposition reaction of electrolytic salt) so as to improve the cell cyclability [36].

The electrochemical impedance spectroscopy (EIS) was used to characterize the impedance properties of $SnS_2$ electrode using different binders after 2 cycles (Fig. 5d). All the Nyquist plots included a semicircle and a linear part, indicating that the electrode reactions were controlled by a mixture of charge transfer and diffusion steps. The semicircle part at high frequencies reflected the charge transfer process and the sloping straight line at low frequencies corresponds to the Li-ion diffusion in the bulk.

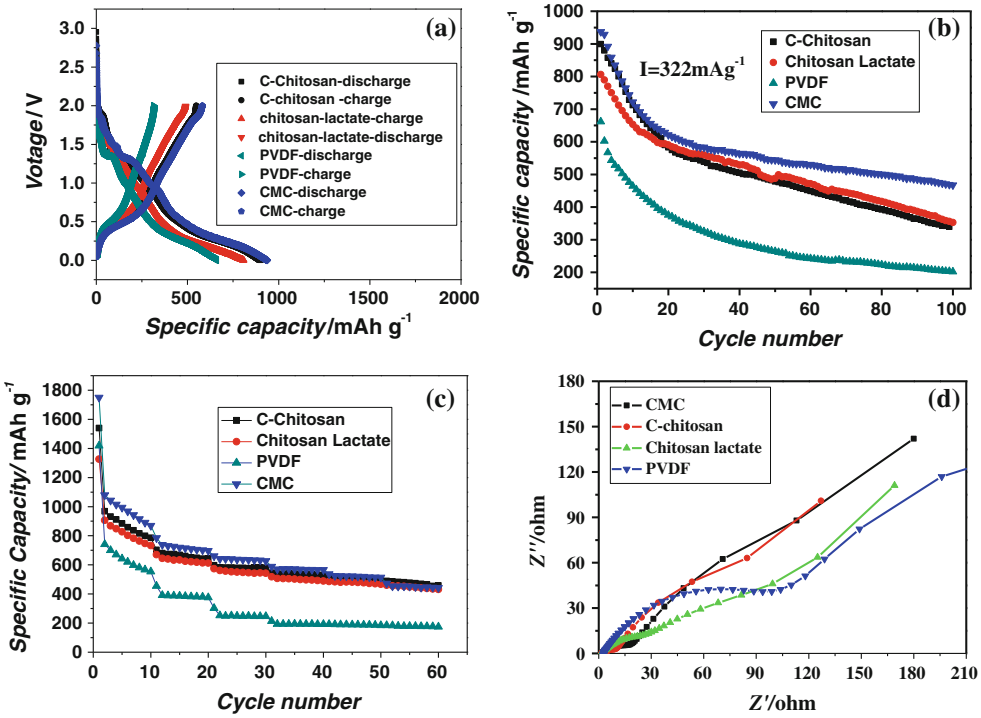


**Fig. 5** The electrochemcial properties of micro/nano-structured $SnS_2$ using different binders. **a** The first charge–discharge curves of $SnS_2$ between 2 and 0 V; **b** the cycling performance at 0.5C rate; **c** the rate capability of $SnS_2$ from 0.1 to 5C; **d** impedance spectra of $SnS_2$ electrode after two cycles

The sum of the charge transfer resistance ($R_{ct}$) and surface film resistance ($R_{sf}$) of $SnS_2$ electrode using C-chitosan, Chitosan lactate, or CMC binder was lower than that of PVDF. The enhanced rate capability could be attributed to an efficient hydrogen bond network formed by the polar groups of the water-soluble polymers and the active particles which facilitated the fast transfer of $Li^+$ ions, and the formation of a stable SEI layer at the surface of $SnS_2$ electrode [37, 38].

## 4 Conclusions

Micro/nano-structured $SnS_2$ with high yield was successfully synthesized through a simple one-pot hydrothermal route. The electrochemical performance of micro/nano-structured $SnS_2$ using the different binders (C-chitosan, Chitosan lactate, CMC, or PVDF) was investigated. Micro/nano-structured $SnS_2$ using water-soluble binders (C-chitosan, Chitosan lactate, CMC) showed higher initial coulombic efficiency, reversible capacity and rate capability, compared with that of PVDF. After 50 cycles at 0.5C rate, the $SnS_2$ electrode using C-chitosan, Chitosan lactate, CMC, and PVDF binder, delivered a discharge specific capacity of 479, 488, 544, and 265 mAh $g^{-1}$, respectively. At a much higher rate of 5C, $SnS_2$ electrode using C-chitosan, Chitosan lactate, CMC, and PVDF binder, exhibited a specific capacity of 458, 432, 442, and 175 mAh $g^{-1}$, respectively. This work shows that chitosan derivatives can serve as a new family of water-soluble binders and potentially replace non-aqueous PVDF binder for LIBs.

**Acknowledgments** This work was supported by the National Science Foundation of China (50973112), the Hundred Talents Program of Chinese Academy of Sciences (CAS), Shenzhen Municipal Special Fund for the Development of Strategic Emerging Industries (JCYJ20120831152211489), and Innovation Fund of GIEC, CAS (y207r41001).

## References

1. Lou XW, Deng D, Lee JY, Feng J, Archer LA (2008) Self-supported formation of needlelike $Co_3O_4$ nanotubes and their application as lithium-ion battery electrode. Adv Mater 20:258–262
2. Wen SH, Hou ZF, Han KLA (2009) Promising anode material for lithium-ion batteries. J Phys Chem C 113:18436–18440
3. Martha SK, Nanda J, Veith GM, Dudney NJ (2012) Electrochemical and rate performance study of high-voltage lithium-rich composition: $Li_{1.2}Mn_{0.525}Ni_{0.175}Co_{0.1}O_2$. J Power Sources 199: 220–226
4. Sladkevich S, Gun J, Prikhodchenko PV, Gutkin V, Mikhaylov AA, Novotortsev VM, Zhu JX, Yang D, Hng HH, Tay YY, Tsakadze Z, Lev O (2012) Peroxide induced tin oxide coating of graphene oxide at room temperature and its application for lithium-ion batteries. Nanotechnology 23:485601
5. Martha SK, Grinblat J, Haik O, Zinigrad E, Drezen T, Miners JH, Exnar I, Kay A, Markovsky B, Aurbach D (2009) $LiMn_{0.8}Fe_{0.2}PO_4$: an advanced cathode material for rechargeable lithium batteries. Angew Chem Int Ed 48:8559–8563
6. Tse KY, Zhang LZ, Baker SE, West R, Hamers RJ (2007) Vertically aligned carbon nanofibers coupled with organosilicon electrolytes: electrical properties of a high-stability nanostructured electrochemical interface. Chem Mater 19:5734–5741
7. Yoo M, Frank CW, Mori S, Yamaguchi S (2003) Effect of poly(vinylidene fluoride) binder crystallinity and graphite structure on the mechanical strength of the composite anode in lithium-ion battery. Polymer 44:4197–4204
8. Guy D, Lestriez B, Guyomard D (2004) New composite electrode architecture and improved battery performance from the smart use of polymers and their properties. Adv Mater 16:553–557
9. Huang H, Yin SC, Kerr T, Taylor N, Nazar LF (2002) Nanostructured composites: a high capacity, fast rate $Li_3V_2(PO_4)_3$/carbon cathode for rechargeable lithium batteries. Adv Mater 14:1525–1528
10. Chen ZH, Christensen L, Dahn JR (2003) Comparison of PVDF and PVDF-TFE-P as binders for electrode materials showing large volume changes in lithium-ion batteries. J Electrochem Soc 150:A1073–A1078
11. Liu WR, Yang MH, Wu HC, Chiao SM, Wu NL (2005) Enhanced cycle life of Si anode for Li-ion batteries by using modified elastomeric binder. Electrochem Solid State Lett 8:A100–A103
12. Li J, Lewis RB, Dahn JR (2007) Sodium carboxymethyl cellulose a potential binder for Si negative electrodes for Li-ion batteries. Electrochem Solid State Lett 10:A17–A20
13. Lee JH, Paik U, Hackney VA, Choi YM (2005) Effect of carboxymethyl cellulose on aqueous processing of natural graphite negative electrodes and their electrochemical performance for lithium batteries. J Electrochem Soc 152:A1763–A1769
14. Drofenik J, Gaberscek M, Dominko R, Poulsen FW, Morgensen M, Pejovnik S, Jamnik J (2003) Cellulose as a binding material in graphitic anodes for Li-ion batteries: a performance and degradation study. Electrochim Acta 48:883–889
15. Lee JH, Paik U, Hackley VA, Choi YM (2006) Effect of poly (acrylic acid) on adhesion strength and electrochemical performance of natural graphite negative electrode for lithium-ion batteries. J Power Sources 161:612–616
16. Li J, Leb DB, Fergusonc PP, Dahna JR (2010) Lithium polyacrylate as a binder for tin–cobalt–carbon negative electrodes in lithium-ion batteries. Electrochim Acta 55:2991–2995
17. Kovalenko I, Zdyrko B, Magasinski A, Hertzberg B, Milicev Z, Burtovyy R, Luzinov I, Yushin G (2011) A major constituent of brown algae for use in high-capacity Li-ion batteries. Science 7:75–79
18. Bridel JS, AzaÏs T, Morcrette M, Tarascon JM, Larcher D (2010) Toward efficient binders for Li-ion battery Si-based anodes: polyacrylic acid. Chem Mater 22:1229–1241
19. Zhai CX, Du N, Zhang H, Yang DR (2011) Large-scale synthesis of ultrathin hexagonal tin disulfide nanosheets with highly reversible lithium storage. Chem Commun 47:1270–1272
20. Luo B, Fang Y, Wang B, Zhou JS, Song HH, Zhi LJ (2012) Two dimensional graphene–$SnS_2$ hybrids with superior rate capability for lithium ion storage. Energy Environ Sci 5:5226–5230
21. Seo JW, Jang JT, Park SW, Kim C, Park B, Cheon J (2008) Two-dimensional $SnS_2$ nanoplates with extraordinary high discharge capacity for lithium-ion batteries. Adv Mater 20:4269–4273
22. Liu Y, Xie JY, Takeda Y, Yang J (2002) Advanced Sn/C composite anodes for lithium-ion batteries. J Appl Electrochem 32:687–692
23. Wang J, Liu J, Xu HB, Ji SM, Wang JB, Zhou YC, Hodgson P, Li YC (2013) Gram-scale and template-free synthesis of ultralong tin disulfide nanobelts and their lithium-ion storage performances. J Mater Chem 1:1117–1122

24. Liu SY, Lu X, Xie J, Cao GS, Zhu TJ, Zhao XB (2013) Preferential c-axis orientation of ultrathin $SnS_2$ nanoplates on graphene as high-performance anode for Li-ion batteries. ACS Appl Mater Interfaces 5:1588–1595
25. Wang QF, Huang Y, Miao J, Zhao Y, Wang Y (2013) Synthesis and electrochemical characterizations of Ce doped $SnS_2$ anode materials for rechargeable lithium-ion batteries. Electrochim Acta 93:120–130
26. Zhong HX, Wang CX (2011) Synthesis and field emission properties of $SnS_2$ and In-doped $SnS_2$ with hierarchical structure. NANO 6:5489–5496
27. Lei YQ, Song SY, Fan WQ, Xing Y, Zhang HJ (2009) Facile synthesis and assemblies of flowerlike $SnS_2$ and $In^{3+}$-doped $SnS_2$: hierarchical structures and their enhanced photocatalytic property. J Phys Chem C 113:1280–1285
28. Zhong HX, Yang GZ, Song HW, Liao QY, Cui H, Shen PK, Wang CX (2012) Vertically aligned graphene-like $SnS_2$ ultrathin nanosheet arrays: excellent energy storage, catalysis, photoconduction, and field-emitting performances. J Phys Chem C 116:9319–9326
29. Price LS, Parkin IP, Hardy AME, Clark RJH (1999) Atmospheric pressure chemical vapor deposition of tin sulfides (SnS, $Sn_2S_3$, and $SnS_2$) on glass. Chem Mater 11:1792–1799
30. Kruk M, Jaroniec M (2001) Gas adsorption characterization of ordered organic–inorganic nanocomposite materials. Chem Mater 13:3169–3183
31. Chen LY, Zhang ZD, Wang WZ (2008) Self-assembled porous 3D flowerlike β-$In_2S_3$ Structures: synthesis, characterization and optical properties. J Phys Chem C 112:4117–4123
32. Hu YS, Adelhelm P, Smarsly BM, Hore S, Antonietti M, Maier J (2007) Synthesis of hierarchically porous carbon monoliths with highly ordered microstructure and their application in rechargeable lithium batteries with high-rate capability. Adv Funct Mater 17:1873–1878
33. Kim TJ, Kim C, Son D, Choi M, Park B (2007) Novel $SnS_2$-nanosheet anodes for lithium-ion batteries. J Power Sources 167:529–535
34. Liu S, Yin XM, Chen L, Li QH, Wang TH (2010) Synthesis of self-assembled 3D flowerlike $SnS_2$ nanostructures with enhanced lithium ion storage property. Solid State Sci 12:712–718
35. Lefebvre-Devos I, Olivier-Fourcade J, Jumas JC, Lavela P (2000) Lithium insertion in $SnS_2$. Phys Rev B 61:3110–3116
36. Zhang SS (2006) A review on electrolyte additives for lithium-ion batteries. J Power Sources 162:1379–1394
37. Lestriez B, Bahri S, Sandu I, Roué L, Guyomard D (2007) On the binding mechanism of CMC in Si negative electrodes for Li-ion batteries. Electrochem Commun 9:2801–2806
38. Wang ZL, Dupre N, Gaillot AC, Lestriez B, Martin JF, Daniel L, Patoux S, Guyomard D (2012) CMC as a binder in $LiNi_{0.4}Mn_{1.6}O_4$ 5 V cathodes and their electrochemical performance for Li-ion batteries. Electrochim Acta 62:77–83